THE JOURNAL OF BIOLOGICAL CHEMISTRY VOL. 289, NO. 16, pp. 11396–11409, April 18, 2014

Proteomic Analysis of Glycine Receptor β Subunit (GlyRβ)-interacting Proteins

*EVIDENCE FOR SYNDAPIN I REGULATING SYNAPTIC GLYCINE RECEPTORS**

Received for publication, July 24, 2013, and in revised form, January 28, 2014 Published, JBC Papers in Press, February 7, 2014, DOI 10.1074/jbc.M113.504860

Isabel del Pino[‡], Dennis Koch[§], Rudolf Schemm[¶], Britta Qualmann[§], Heinrich Betz[‡‖1], and Ingo Paarmann[‡2]

From the [‡]Department of Neurochemistry, Max-Planck-Institute for Brain Research, D-60438 Frankfurt/Main, the [§]Institute for Biochemistry I, Jena University Hospital, Friedrich Schiller University Jena, D-07743 Jena, the [¶]Department for Theoretical and Computational Biophysics, Max-Planck-Institute for Biophysical Chemistry, D-37077 Göttingen, and the [‖]Max-Planck Institute for Medical Research, 69120 Heidelberg, Germany

Background: Glycine receptors mediate inhibitory neurotransmission in the central nervous system.
Results: Syndapin I is a new interaction partner of the glycine receptor β subunit, and its down-regulation reduces synaptic glycine receptor levels.
Conclusion: Syndapin I is involved in glycine receptor trafficking to and/or anchoring at inhibitory postsynapses.
Significance: Disclosing new determinants of glycine receptor clustering is crucial for understanding inhibitory synapse formation.

Glycine receptors (GlyRs) mediate inhibitory neurotransmission in spinal cord and brainstem. They are clustered at inhibitory postsynapses via a tight interaction of their β subunits (GlyRβ) with the scaffolding protein gephyrin. In an attempt to isolate additional proteins interacting with GlyRβ, we performed pulldown experiments with rat brain extracts using a glutathione *S*-transferase fusion protein encompassing amino acids 378–455 of the large intracellular loop of GlyRβ as bait. This identified syndapin I (SdpI) as a novel interaction partner of GlyRβ that coimmunoprecipitates with native GlyRs from brainstem extracts. Both SdpI and SdpII bound efficiently to the intracellular loop of GlyRβ *in vitro* and colocalized with GlyRβ upon coexpression in COS-7 cells. The SdpI-binding site was mapped to a proline-rich sequence of 22 amino acids within the intracellular loop of GlyRβ. Deletion and point mutation analysis disclosed that SdpI binding to GlyRβ is Src homology 3 domain-dependent. In cultured rat spinal cord neurons, SdpI immunoreactivity was found to partially colocalize with marker proteins of inhibitory and excitatory synapses. When SdpI was acutely knocked down in cultured spinal cord neurons by viral miRNA expression, postsynaptic GlyR clusters were significantly reduced in both size and number. Similar changes in GlyR cluster properties were found in spinal cultures from SdpI-deficient mice. Our results are consistent with a role of SdpI in the trafficking and/or cytoskeletal anchoring of synaptic GlyRs.

Postsynaptic inhibition by glycine is mediated by strychnine-sensitive glycine receptors (GlyRs),[3] ligand-gated chloride channels of the Cys loop receptor family (1). GlyRs are composed of α and β subunits (2, 3), which assemble into homomeric α-pentamers or $\alpha_2\beta_3$ heteromeric receptors (4). Each subunit consists of an extended N-terminal extracellular domain, four transmembrane domains, and a large intracellular loop between transmembrane domains 3 and 4. The β subunit (GlyRβ) provides for synaptic localization of the GlyRs by interacting with the postsynaptic scaffolding protein gephyrin (5, 6). The gephyrin-binding motif (GBM) of GlyRβ is located in the large intracellular loop and has been shown to also be important for the anterograde and retrograde dendritic transport of GlyRs, in which gephyrin functions as an adaptor for kinesin-5 and the dynein light chains 1 and 2 (Dlc1/2), respectively (7–9). In addition to gephyrin, the trafficking proteins vacuolar protein sorting 35 (Vps35) and neurobeachin (Nbea) have been recently found to interact with GlyRβ involving loop residues adjacent to the GBM (10). Notably, the GlyRβ loop sequence is predicted to also contain Src homology 3 (SH3) domain ligand-binding motifs (SBMs) (1), suggesting that SH3 domain containing proteins might be implicated in the cell biology of synaptic GlyRs.

SH3 domain proteins are involved in endocytosis and actin remodeling (11). Syndapins (Sdps) are SH3 domain containing proteins found in all multicellular eukaryotes and belong to the family of Fes/CIP4 homology Bin-Amphiphysin-Rvs (F-BAR) proteins (12). F-BAR domains can dimerize, bind negatively

* This work was supported by the Max Planck Society (to H. B.), Deutsche Forschungsgemeinschaft Grants PA1623/2-1, Qu116/5-1, and -5-2, Schram-Stiftung (to B. Q.), and Fonds der Chemische Industrie (to H. B.).
[1] To whom correspondence may be addressed: Max-Planck Institute for Medical Research, Jahnstrasse 29, 69120 Heidelberg, Germany. Tel.: 49-6221-486453; E-mail: heinrich.betz@mpimf-heidelberg.mpg.de.
[2] To whom correspondence may be addressed: Blumenweg 34, D-73447 Oberkochen, Germany. Tel.: 49-73447-2900643; E-mail: Ingo.Paarmann@gmx.net.

[3] The abbreviations used are: GlyR, glycine receptor; COS-7, African Green Monkey SV40-transformed kidney fibroblast cell line; DIV, day *in vitro*; Dlc, dynein light chain; ELM, eukaryotic linear motif; ER, endoplasmic reticulum; F-BAR, Fes/CIP4 homology Bin-Amphiphysin-Rvs; GAD67, glutamate decarboxylase isoform 67; GBM, gephyrin-binding motif; GlyRβ, β subunit of the glycine receptor; MBP, maltose-binding protein; mRFP, monomeric red fluorescent protein; Nbea, neurobeachin; NPF, asparagine/proline/phenylalanine; N-WASP, neural Wiskott-Aldrich syndrome protein; PSD-95, postsynaptic density protein 95; Sdp, Syndapin; SH3, Src homology 3; SBM, Src homology 3 domain ligand-binding motif; VIAAT, vesicular inhibitory amino acid transporter; Vps35, vacuolar protein sorting 35.

charged lipids, such as phosphatidylserine and phosphatidylinositol 4,5-bisphosphate, and sculpt membranes (13). At the C terminus, Sdps contain an SH3 domain, which interacts with the GTPase dynamin and other proteins involved in vesicular transport. Of the three Sdp isoforms, SdpI is expressed in brain, SdpII ubiquitously, and SdpIII in skeletal muscle, heart, lung, and weakly in brain (14). Sdps have been implicated in vesicle formation at the plasma membrane, the trans-Golgi network, and the recycling endosome, as well as in actin polymerization (14–19). In SdpI-deficient ($SdpI^{-/-}$) mice, synaptic vesicle endocytosis is significantly impaired, resulting in enhanced hippocampal network activity and seizures (20). Notably, in $SdpI^{-/-}$ neurons evoked inhibitory postsynaptic currents are more severely reduced than the excitatory ones, suggesting a specific role in inhibitory neurotransmission of this Sdp isoform (20).

In an attempt to identify novel GlyRβ-binding proteins that interact with the predicted SBMs and might be implicated in the molecular organization of inhibitory glycinergic postsynapses, we performed proteomic screens using a glutathione *S*-transferase (GST) fusion protein containing amino acids 378–455 of GlyRβ, *i.e.* the C-terminal portion of its large intracellular loop. Here, we report that SdpI and the two known splice variants of SdpII interact with the GlyRβ loop by recognizing an SBM that lies adjacent to but does not include the GlyRβ 378–426 region. Mapping experiments revealed that the SBM of GlyRβ interacts with the SH3 domain of SdpI. Upon miRNA-mediated knockdown of SdpI in cultured rat spinal cord neurons, we observed a reduction in both the size and number of postsynaptic GlyR clusters. Similar results were obtained with spinal cord cultures prepared from $SdpI^{-/-}$ mice. Our data indicate that SdpI participates in the trafficking and/or cytoskeletal anchoring of synaptic GlyRs.

EXPERIMENTAL PROCEDURES

GST Pulldowns—GlyRβ(378–455), GlyRβ(403–455), GlyRβ(427–455), GlyRβ(427–448), GlyRβ(378–440), GlyRβ(378–440)/P429A, GlyRβ(378–455)/P441A, GlyRβ(378–455)/PPAA (P438A/P441A double mutation), and GlyRβ(378–455)/KKAA (K434A/K435A double mutation) were cloned by standard PCR protocols, using rat GlyRβ-pBluescript (3) as template, into pGEX-RB (21), GlyRβ(378–426) and GlyRβ(378–455) additionally into pMal-TEV (22). GlyRβ(378–426)-pGEX-RB has been described previously (10). The gephyrin-E domain was cloned from gephyrin-E domain-pRSET (23) into the pGEX-4T-1 vector (GE Healthcare). The SdpI, $SdpI_{P434L}$, $SdpI_{\Delta SH3}$, $SdpI_{SH3}$, $SdpI_{SH3/P434L}$, SdpII-l, and SdpII-s constructs have been described previously (15, 24). SdpI, $SdpI_{P434L}$, $SdpI_{\Delta SH3}$, SdpII-l, and SdpII-s were cloned into the pRSETA vector (Invitrogen) providing a His_6 tag, and all SdpI constructs additionally into the pGEX-4T-1 vector using BamHI and EcoRI restriction sites. GST was expressed from pGEX-RB, when used as control for GlyRβ constructs in pGEX-RB, and from pGEX-4T-1 for the other constructs. The sequences of all expression constructs were confirmed by DNA sequencing (Eurofins MWG GmbH, Ebersberg, Germany).

His_6-tagged Sdp constructs were expressed in *Escherichia coli* C41 DE3 (25) and all other constructs in *E. coli* BL21 DE3 (Merck). Expression and preparation of clear lysates were performed as described previously (26).

GST pulldowns of recombinant proteins were done as described previously (10); a mouse monoclonal α-His_6 antibody (1:1000, Merck) was used for Western blotting. The binding activity of GST-GlyRβ constructs containing the GBM was monitored by pulldown of the His_6-tagged E-domain of gephyrin. All GST pulldown experiments were repeated three times. The GST pulldowns for isolation of GlyRβ-interacting proteins from brain extracts using GlyRβ(378–455), the preparation of tissue extracts, SDS-PAGE separation and mass spectrometry (MS) were carried out as described for GlyRβ(378–426) (10, 26).

Coimmunoprecipitation—Detergent extracts were prepared from brainstems of adult (4 months old) C57BL/6 mice by homogenizing the tissue at a w/v ratio of 1:3 in lysis buffer (20 mM HEPES, pH 7.5, 100 mM KCl, 5 mM EGTA, 5 mM $MgCl_2$ and 50 mM NaCl) supplemented with 1% (w/v) Triton X-100, 5 mM DTT, and complete protease inhibitor mixture (1 tablet/50 ml; Roche Diagnostics) using a Dounce homogenizer. The homogenate was left for 1 h on an overhead rotator at 4 °C and centrifuged at 10,000 × *g* for 10 min. The resulting supernatants were pre-cleared by incubation with protein A- or protein G-Sepharose for 1 h. Affinity-purified anti-SdpI from guinea pig (16) or unrelated guinea pig IgGs was immobilized on protein A-Sepharose (Sigma), and mAb4 or unrelated mouse IgGs were immobilized on protein G-Sepharose (Sigma) in the presence of 5% (w/v) bovine serum albumin. After three washes with lysis buffer containing 1% (w/v) Triton X-100, the resin was incubated overnight with 0.8–1.0 ml of pre-cleared brainstem homogenate at a concentration of 2 mg of protein/ml. After five washes with 1% (w/v) Triton X-100-containing lysis buffer, bound proteins were eluted with SDS sample buffer and analyzed by SDS-PAGE and immunoblotting.

TAT Peptide Competition Experiments—All peptides used contained an N-terminal fluorescein conjugate and the TAT sequence as shown by underlines, and the amino acids important for SdpI binding are shown in italics as follows: TAT-GlyRβ_{22}, YGRKKRRQRRRGKPQAKN*KK*PP*P*AK*P*VIPTAAK; TAT-scrambled, YGRKKRRQRRRAQKVAPGPITKPKPNPAKAPKK. The TAT-scrambled peptide contains the same amino acids as TAT-GlyRβ_{22}, but the GlyRβ residues are randomly ordered, and no SBM is present. Peptides were purchased from Biosyntan GmbH, Berlin, Germany, and had a purity of at least 95%. GST pulldowns were performed as explained above, except that TAT-GlyRβ_{22} was added in concentrations of 1–100 μM during the incubation of GST-GlyRβ(378–455) with His_6-SdpI. TAT-scrambled was used as control.

Molecular Modeling—The SdpI-GlyRβ model was generated by Modeler9 version 5-1 (27) using the x-ray structure 2DRM and the nuclear magnetic resonance solution structure 1RLQ as templates for the rat SdpI SH3 domain and the rat GlyRβ SBM, respectively. After energy minimization, the model was subjected to a 50-ns molecular dynamics simulation run. The simulation was run with Gromacs (28), version 4.6, and the following parameters: amber03 (29) all-atom force field, tip4p water model, and 0.15 M concentrations of Na^+ and Cl^- ions. From the whole trajectory an average structure was generated, which was energy-minimized (steepest descent, 800 ps) subsequently.

Endoplasmic Reticulum (ER) Retention Assay—Myc-tagged SdpII constructs in pCMV-Tag3B and Myc-tagged SdpI in pRK5 have been described previously (30). Monomeric red fluorescent protein (mRFP)-GlyRβ was generated from green fluorescent protein (GFP)-GlyRβ and mRFP-gephyrin (kindly provided by Matthias Kneussel (8)) by replacing the GFP tag with mRFP amplified by PCR from mRFP-gephyrin. The 3′-UTR was removed by PCR using EcoRV and HindIII restriction sites. GFP was expressed from peGFP-C2 (Clontech). Myc-Dlc1, GFP-gephyrin, and GFP-gephyrin$_{mut}$ unable to bind GlyRβ have been described (7, 23). pDsRed2-ER (Clontech) was used to visualize the ER. African Green Monkey SV40-transformed kidney fibroblasts (COS-7 cells) were cultured on glass coverslips and transfected using Lipofectamine™ 2000 (Invitrogen) following the manufacturer's instructions. Twenty four hours after transfection, cells were fixed with 4% (w/v) paraformaldehyde in phosphate-buffered saline (PBS) for 5–10 min, permeabilized with 0.5% (v/v) IgePal (Sigma) for 30 min, and blocked with 10% (v/v) goat serum in PBS for 1 h. Antibody staining was performed by incubation for 1 h with primary antibodies and 45 min with secondary antibodies in blocking solution. The following antibodies were used: rabbit α-Myc antibody (Santa Cruz Biotechnology, Inc., Heidelberg, Germany; 1:1000) and Alexa-488 goat α-rabbit (Molecular Probes, Eugene, OR; 1:1000).

SdpI Knockdown—pAAV-6P-SEWB was a gift of Sebastian Kügler (Göttingen, Germany) and provides a neuron-specific synapsin promoter (31). siRNA-resistant Myc-SdpI-siR (32) was cloned via NheI-HindIII sites into pAAV-6P-SEWB. The pDP1rfps and pDP2rfps plasmids (33) were provided by Jürgen Kleinschmidt (Heidelberg, Germany). Primers TGCTGTC-CTCGTTCAGTAGGCTGTTCGTTTTGGCCACTGACTG-ACGAACAGCCCTGAACGAGGA (sense) and CCTGTC-CTCGTTCAGGGCTGTTCGTCAGTCAGTGGCCAAAA-CGAACAGCCTACTGAACGAGGAC (antisense) were designed for shRNAmiR according to Invitrogen's instructions based on the SdpI-siRNA sequence (32) GAACAGCCTACT-GAACGAG (underlined sequences of sense and antisense primers are derived from the siRNA sequence). Primers were annealed and cloned into pcDNA6.2-GW-EmGFP-miR in line with the manufacturer's instructions (Invitrogen). A control miRNA construct was provided by Invitrogen. The GFP-shRNAmiR regions of both constructs were cloned into pAAV-6P-attR (gift from Sebastian Kügler (Göttingen, Germany)) containing a synapsin promoter by recombination using BP-clonase II, pDONR221, and LR-clonase II (Invitrogen) according to the manufacturer's protocol. Plasmids control-miR-pAAV-6P-attR (control-miR), SdpI-miR-pAAV-6P-attR (SdpI-miR), and rescue construct Myc-SdpI-siR-pAAV-6P (SdpI-siR) were individually cotransfected with pDP helper plasmids (pDP1 and pDP2) in equimolar amounts. Transfection into human embryonic kidney 293T cells was achieved by calcium phosphate transfection as described previously (33). Forty eight hours after transfection, the cells were collected, and packaged viruses were released into 50 mM Tris, pH 8.0, 150 mM NaCl by three cycles of freeze-thawing on dry ice/ethanol. Viruses were purified by iodixanol density centrifugation as described previously (34) and concentrated using a 100-kDa cutoff Amicon centrifugal filter unit (Millipore, Schwalbach, Germany). Infectious unit titers were determined in rat primary neuron cultures for each recombinant adeno-associated virus preparation. Equivalent infectious units of the control-miR and SdpI-miR were diluted in 10 μl of PBS and added to the medium of spinal cord neuron cultures at day *in vitro* (DIV) 7. For rescue experiments, cultures were infected with a mixture of 10 μl of SdpI-miR and 10 μl of Myc-SdpI-siR. By DIV21, neurons were washed with PBS and either harvested in PBS for Western blot analysis or fixed for immunostaining.

Immunofluorescence Staining—Cultures of dissociated mouse (C57BL/6) and rat (Wistar; Charles River, Sulzfeld, Germany) spinal cord neurons were prepared from embryonic day 14.5 embryos and maintained as described previously (35). SdpI$^{-/-}$ mice were bred in the C57BL/6 background and genotyped as detailed previously (20). When comparing results obtained with WT and SdpI$^{-/-}$ embryos or mice, both genotypes were always derived from the same litter. The protocols used for culturing and immunostaining dissociated spinal cord neurons from rat have been published previously (10). Immunohistochemistry on brainstem slices prepared from adult mice was performed as described previously (36). Quantifications of cluster densities and sizes were performed on 140–400 clusters per condition/genotype in spinal cord cultures and 6000–10,000 clusters per genotype in brain slices, respectively.

Antibodies Used for Immunostaining—mAb4a recognizing primarily GlyRα subunits (1:250) and mAb7 specific for gephyrin (1:400) have been characterized previously (37, 38). Monoclonal antibodies against postsynaptic density protein-95 (PSD-95; Affinity Bioreagents, Golden, CO; 1:200), vesicular inhibitory amino acid transporter (VIAAT; also named vesicular γ-aminobutyric acid (GABA) transporter, VGAT) (Synaptic Systems GmbH, Göttingen, Germany; 1:1000), and glutamic acid decarboxylase-67 (GAD67; Chemicon International, Temecula, CA), as well as polyclonal rabbit antibodies against SdpI (SdpI-2704; 1:1000 (24)) and VIAAT (Synaptic Systems GmbH, Göttingen, Germany; 1:1000–1:4000) were also employed. Species-specific Alexa-488-, Alexa-546-, and Alexa-635-conjugated secondary antibodies were purchased from Molecular Probes (Eugene, OR; 1:1000). Monoclonal antibody against β3-tubulin (1:1000) was obtained from HiSS Diagnostics GmbH, Freiburg, Germany.

Immunofluorescence and Image Analysis—GFP, DsRed2, and mRFP were visualized by endogenous fluorescence. For colocalization analysis, images were obtained using an AxioImager microscope equipped with an ApoTome (Zeiss, Göttingen, Germany). In the ER retention assay, the areas colocalizing in merged images were normalized to the areas in the red channel. Co-localization experiments of SdpI puncta with synaptic markers in rat spinal cord neurons were performed as described previously (10). For the quantification of punctate immunofluorescence (density and average size of synaptic clusters), images of immunostained spinal cord neurons were captured as described previously (39), and 50 μm neuritic segments emanating from the somata were marked and evaluated. Binarization, thresholding, and quantification were performed with the ImageJ 1.42q software (National Institutes of Health, Bethesda). If not indicated otherwise, quantitative data repre-

sent means ± S.E. from 30 randomly selected cells (10 per independent experiment). Statistical significance was evaluated with two-tailed Student's *t* test for paired comparisons and analysis of variance with post hoc Bonferroni correction for multiple comparisons.

RESULTS

Sdps Interact with GlyRβ—In an attempt to search for novel GlyRβ-binding proteins, we employed a fragment of the GlyRβ loop that included its predicted SBMs (residues 378–455) in GST pulldown experiments with rat brain detergent extracts, as used previously for identifying the GlyRβ interaction partners Vps35 and Nbea (10). Fig. 1*A* shows that GST-GlyRβ(378–455) but not GST reproducibly isolated a protein band with an apparent molecular mass of about 52 kDa that had not been detected in previous screens with GST-GlyRβ(378–426) (10, 26). By matrix-assisted laser desorption/ionization-time of flight spectrometry, this protein was identified as SdpI (Table 1). A representative mass spectrum in its deisotopized form is shown in Fig. 1*B*.

To confirm our MS results and to also test for direct interaction, we performed GST pulldown experiments with the recombinant proteins. Fig. 1*C* shows that GST-GlyRβ(378–455) and His_6-SdpI interacted strongly, whereas no binding of SdpI to GST-GlyRβ(378–426), which lacks the last 29 amino acids of GlyRβ(378–455), could be detected. Similarly, both the long and the short splice variants of SdpII (SdpII-l and SdpII-s) cosedimented with GST-GlyRβ(378–455) but not GST-GlyRβ(378–426) (Fig. 1*D*). Thus, GlyRβ binding is a property not restricted to SdpI but shared by other Sdp isoforms.

To examine whether the interaction also occurs between native GlyRs and SdpI, we performed coimmunoprecipitation experiments with detergent extracts from adult mouse brainstem. Antibodies against SdpI precipitated not only their native antigen (data not shown) but also GlyRα immunoreactivity (Fig. 1*E*). Inversely, a monoclonal antibody against GlyRα (mAb4a) coisolated SdpI (Fig. 1*F*). These results indicate that native GlyRs present in brainstem extracts interact with SdpI.

Identification of SdpI- and GlyRβ-binding Sites—SdpI consists of an N-terminal F-BAR domain, followed by a region containing NPF motifs, and a C-terminal SH3 domain (Fig. 2*A*). To delineate whether the SH3 domain of SdpI is involved in GlyRβ binding, we introduced a point mutation known to interfere with binding of the SH3 domain to its ligands, $SdpI_{P434L}$ (24), and also deleted the SH3 domain in the $SdpI_{\Delta SH3}$ construct (Fig. 2*A*). GST pulldowns disclosed that the binding of both $SdpI_{P434L}$ and $SdpI_{\Delta SH3}$ to GST-GlyRβ(378–455) was almost completely abrogated as compared with wild type (WT) SdpI (Fig. 2*B*). This indicates that an intact SH3 domain of SdpI is essential for tight interaction. To confirm this result, we used an inverted GST pulldown with GST-tagged SdpI constructs and maltose-binding protein (MBP)-tagged GlyRβ constructs. We found that both full-length SdpI and the isolated SH3 domain of SdpI, but neither the SH3 domain with the P434L point mutation, the full-length SdpI with this mutation, nor SdpI without the SH3 domain, were able to bind MBP-GlyRβ(378–455) (Fig. 2*C*). To exclude false positive results due to the presence of the

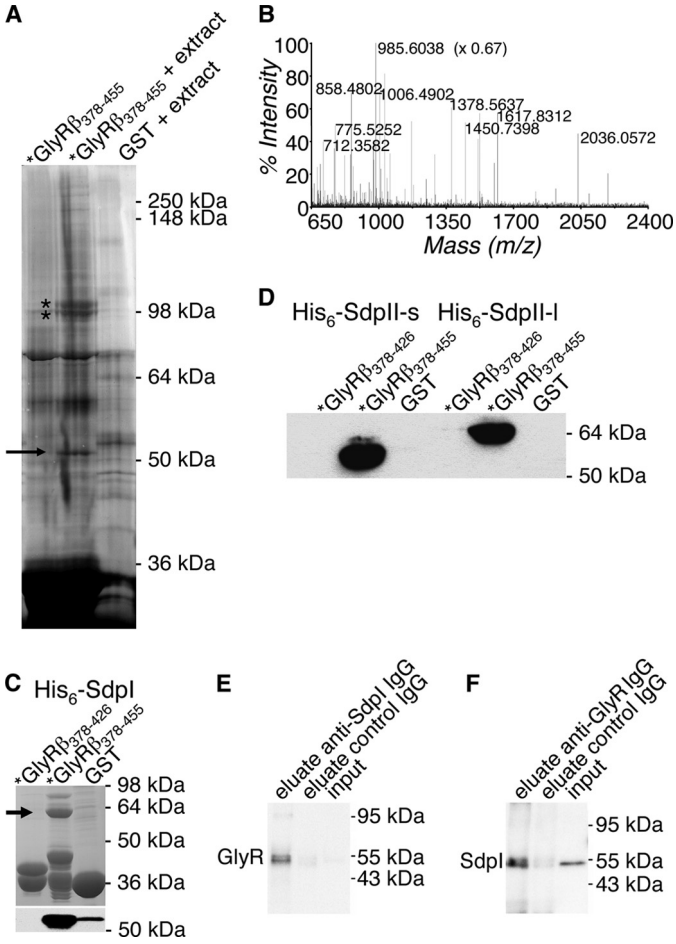

FIGURE 1. **Sdps interact with GlyRβ.** *A,* pulldown by GST-GlyRβ(378–455) of a protein with an apparent molecular mass of 52 kDa from rat brain detergent extract. Lanes show proteins isolated by glutathione-Sepharose beads and detected by silver staining from the following incubations: *1st lane*, GST-GlyRβ(378–455) with buffer only; *2nd lane*, GST-GlyRβ(378–455) with brain extract; *3rd lane*, GST with brain extract. The *arrow* points to a 52-kDa band present in the *2nd lane* only; the bands at ~98 kDa, marked with *asterisks*, also present in this lane likely represent gephyrin splice variants (26). *B,* representative mass spectrum for the protein band at 52 kDa found in *A*. The protein was identified as SdpI. Major SdpI peaks are indicated by their molecular masses. The 985.6038-Da peak was scaled down by 0.67. *C,* GST pulldown of recombinantly expressed His_6-SdpI. Proteins were isolated and visualized by Coomassie Blue staining: *left lane,* GST-GlyRβ(378–426); *middle lane,* GST-GlyRβ(378–455); *right lane* (*GST*). The *arrow* points to the position of His_6-SdpI bound by GST-GlyRβ(378–455). The 80-kDa band seen in the *middle lane* is the *E. coli* DnaK protein as identified by MS, a common contamination when dealing with GST fusion proteins. The bands in the 28–40-kDa range are the GST fusion proteins. Double bands for GST-GlyRβ(378–426) and GST-GlyRβ(378–455) resulted from partial cleavage of the GST fusion proteins. Upon Western blotting and subsequent immunodetection with the anti-His_6 antibody, weak binding to GST was observed in this experiment (*bottom panel, right lane*). *D,* immunodetection of GST pulldowns of His_6-tagged SdpII-s (*first three lanes*) and SdpII-l (*last three lanes*) obtained with the indicated GST fusion proteins. Both the long and the short splice variant of SdpII interact with GlyRβ(378–455) but not with the shorter fragment GST-GlyRβ(378–426) and the negative control GST. *, GST. *E,* coimmunoprecipitation of GlyRα immunoreactivity from brainstem detergent extract by anti-SdpI; for immunodetection, mAb4 was used. *Left lane,* eluate from anti-SdpI beads; *middle lane,* eluate from control IgG beads; *right lane,* input. Note that GlyR was hardly detectable in the input fraction and control IgG eluate but strongly detected in the anti-SdpI eluate. *F,* coimmunoprecipitation of SdpI immunoreactivity from brainstem detergent extract by anti-GlyR (mAb4); for immunodetection, anti-SdpI was used. Note prominent SdpI band in the eluate from the anti-GlyR beads.

MBP tag, binding of MBP-GlyRβ(378–426) was also tested. We detected a strong binding of MBP-GlyRβ(378–426) to gephyrin, showing that the protein fragment is properly folded

TABLE 1

Identification of SdpI by mass spectrometry

Proteins with an apparent molecular mass of 52 kDa from three independent experiments were analyzed by MALDI-TOF mass spectrometry. Sequence coverage at the amino acid level and accuracy of the measurements are indicated (ppm, parts per million). *p*, the probability that the observed match of the mass spectrum with SdpI from the database is a random event, is also given. Additionally, the number of peptides matching SdpI is indicated. Of the different Sdp isoforms detected, SdpI is the only isoform detected in all three pulldown experiments analyzed. Of the few peptides corresponding to SdpII and SdpIII, only two are clearly not derived from SdpI.

Experiment	1	2	3
Sequence coverage	30%	45%	37%
Accuracy	22 ppm	25 ppm	20 ppm
p	$5{\cdot}10^{-12}$	$5{\cdot}10^{-15}$	$5{\cdot}10^{-12}$
No. of analyzed peaks	33	75	44
No. of peptides without contaminant masses	23	62	31
SdpI peptides	13	24	15
SdpII peptides	0	6	1
SdpIII peptides	0	3	2

but not to any of the SdpI constructs (Fig. 2*C*). Together, these results indicate that an intact SH3 domain is both necessary and sufficient for the binding of SdpI to GlyRβ(378–455).

The binding site of SdpI within GST-GlyRβ(378–455) was mapped using a deletion approach. Stepwise removal of the first 50 amino acids, including the GBM (GST-GlyRβ(403–455) and GST-GlyRβ(427–455)), did not affect SdpI binding (Fig. 2*D*). A construct lacking the last 15 amino acids of GlyRβ(378–455), including a part of the SBM (GST-GlyRβ(378–440)), exhibited a slightly reduced binding. We observed that 22 amino acids from position 427 to 448 containing the entire SBM were sufficient for a strong interaction (Fig. 2*D*). This result was confirmed by peptide competition (Fig. 2*E*). A TAT peptide corresponding to sequence 427–448 of GlyRβ, TAT-GlyRβ_{22}, but not a TAT peptide containing the same amino acids but randomly ordered (TAT scrambled), inhibited SdpI binding to GST-GlyRβ(378–455). This result shows that the interaction between the cytosolic loop of GlyRβ and the SH3 domain of SdpI is sequence-specific.

GlyRβ Point Mutations Interfering with SdpI Binding—The results presented above (summarized in Fig. 3*A*) suggested an SH3-SBM-type interaction (40) for SdpI binding to GlyRβ. Eukaryotic linear motif (ELM) (41) predicts at least two independent SH3 ligand-binding motifs, KP*XX*K and K*XX*P*XX*P, within the above defined SdpI-binding site (amino acids 427–448) of GlyRβ(378–455). Within the last 15 amino acids, whose removal reduced SdpI binding (positions 441–455; Fig. 3*A*), Pro-441 is, according to ELM prediction, essential for SH3 interaction. Hence, we mutated this residue to alanine. In addition, ELM identified Pro-429 as potentially also important for SH3 domain-ligand interactions in the remainder of the SBM (Fig. 3*A*). Therefore, we also replaced this proline by an alanine in GST-GlyRβ(378–440), which lacks the last 15 residues of GST-GlyRβ(378–455) but still exhibited SdpI binding. Fig. 3*B* (*left panel*) shows that neither the P441A mutation nor the P429A substitution abolished the interaction (Fig. 3*B*).

In a typical (R/K)*XX*P*XX*P SH3 ligand-binding motif, Arg/Lys provides additional binding energy through electrostatic interactions (40). Amino acid sequence analysis revealed the presence of such a motif in the SBM of GlyRβ, *i.e.* residues Lys-435, Pro-438, and Pro-441. Therefore, we designed double point mutations to examine its importance. The GST-GlyR$\beta_{P438A/P441A}$ (PPAA) double substitution led to a dramatic decrease in SdpI binding. For Lys-435, a double mutant K434A/K435A (KKAA) was created to avoid compensatory effects due to the neighboring Lys-434 (Fig. 3*A*); this led to a complete loss of SdpI binding (Fig. 3*B*). To demonstrate that this result was specifically due to the substitutions introduced and not caused by more general conformational effects, all aforementioned deletion and mutant constructs were examined for gephyrin binding. Fig. 3*B* (*lower panels*) shows that gephyrin interacted with all fusion proteins examined to a similar extent as found with GST-GlyRβ(378–455). Taken together, these results indicate that the K*XX*P*XX*P motif is indeed the SdpI-binding site.

To better understand how GlyRβ interacts with SdpI, we made an attempt to model the regions involved based on known

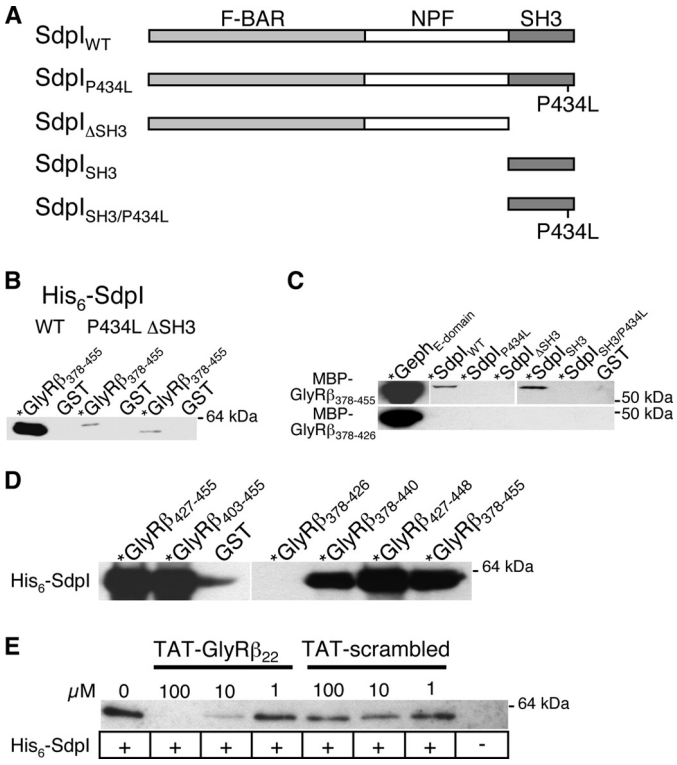

FIGURE 2. **Localization of the binding sites of GlyRβ and SdpI.** *A,* domain structure of SdpI. The N-terminal F-BAR and the C-terminal SH3 domains are connected by a flexible region containing two NPF motifs. Point and deletion mutants used are shown below the WT protein. *B,* immunodetection of GST pulldowns of His$_6$-tagged SdpI WT (*1st* and *2nd lane*), SdpI$_{P434L}$ (*3rd* and *4th lane*), and SdpI$_{\Delta SH3}$ (*5th* and *6th lane*) by GST-GlyRβ(378–455), and as negative control GST. Similar amounts of the three SdpI proteins were used. An intact SH3 domain is essential for robust interaction of SdpI with GST-GlyRβ(378–455), as indicated by strong binding of SdpI WT only. *, GST. *C,* immunodetection of MBP-tagged GlyRβ fragments coprecipitated with GST-tagged SdpI constructs. *Top row,* MBP-GlyRβ(378–455) interacts with full-length SdpI and the SH3 domain of SdpI but not with SdpI$_{P434L}$, SdpI$_{\Delta SH3}$, SdpI$_{SH3/P434L}$, or GST. *Bottom row,* With MBP-GlyRβ(378–426), no binding to SdpI constructs was observed. Gephyrin binding served as positive control, because the GBM is present in both GlyRβ fragments. *, GST. *D,* mapping of the SdpI-binding site in GlyRβ. SdpI bound strongly to all GST-GlyRβ constructs containing amino acids 427–448; deletion of amino acids 441–448 weakened the interaction. GST and GlyRβ(378–426) were used as negative controls. *E,* TAT peptide encompassing residues 427–448 of GlyRβ (TAT-GlyRβ_{22}) inhibited the pulldown of His$_6$-SdpI by GST-GlyRβ(378–455), whereas a respective control peptide (TAT-scrambled) did not, as revealed by immunodetection of bound His$_6$-SdpI. Peptide concentrations included are indicated above, and the presence of His$_6$-SdpI is indicated below the individual immunoreactive bands.

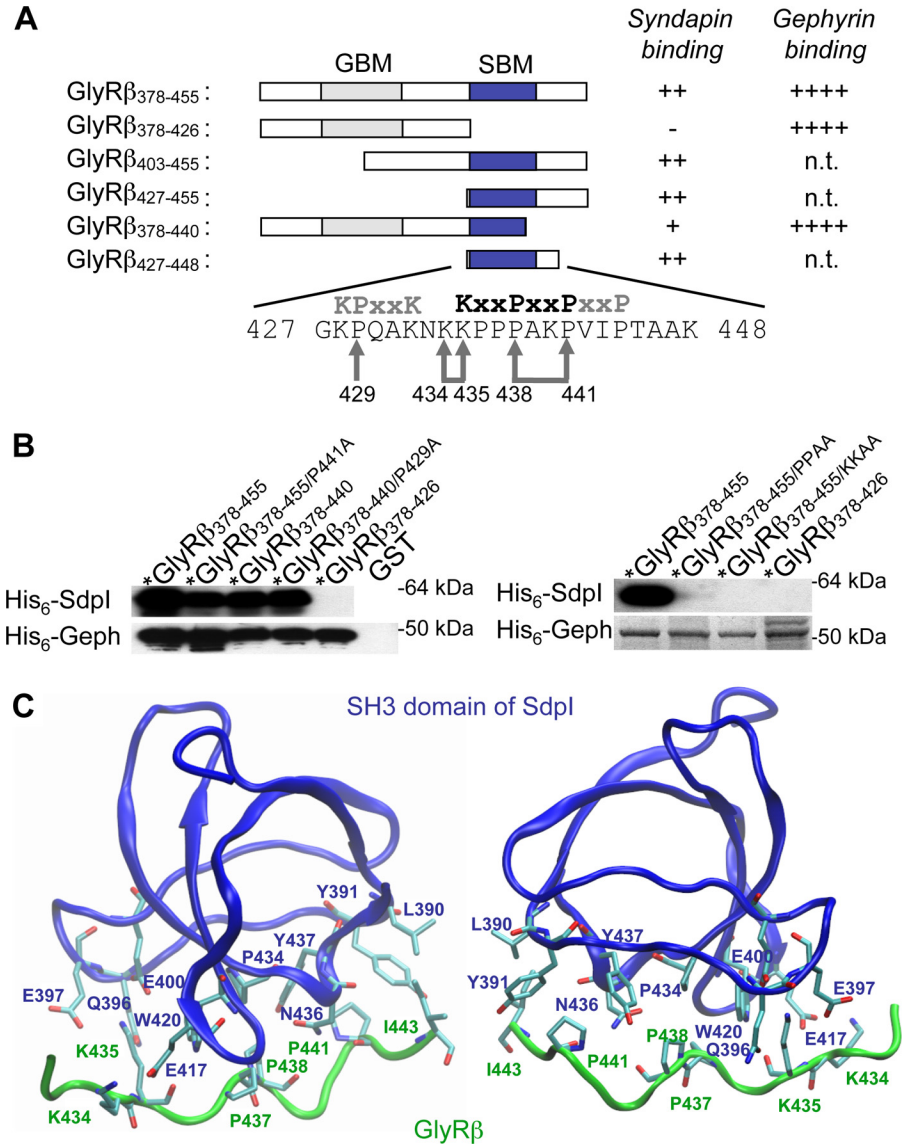

FIGURE 3. **Consensus SBM sequence in the GlyRβ loop mediates SdpI binding.** *A,* summary of the deletion mapping results shown in Figs. 1 and 2. The relative strength of SdpI and gephyrin binding to the different constructs is indicated by the number of symbols: ++++, very strong; ++, intermediate; +, weak binding; −, no binding; *n.t.*, not tested. The minimal SdpI binding region localized to positions 427–448 contains multiple proline and lysine residues, out of which Pro-429, Lys-434, Lys-435, Pro-438, and Pro-441 were mutated to alanine. *Simple arrows* point to mutated residues and *linked arrows* to double mutations. *B,* identification of point mutations interfering with SdpI binding by GST pulldown. *Top row,* immunodetection of His_6-SdpI binding to the indicated GST fusion proteins, with GST serving as a negative control. *Bottom row,* gephyrin binding to the same fusion constructs (immunodetection shown in *left lower panel*, and Coomassie staining in *right lower panel*). Both the P441A single substitution and the P429A mutation had no major effect on SdpI binding. The K434A/K435A (KKAA) double mutation abolished the interaction with SdpI, and the P438A/P441A (PPAA) double mutation reduced it significantly. Gephyrin binding was not affected by the double mutations. * indicates N-terminally fused GST. *C,* model for the interaction of GlyRβ and SdpI. The SH3 domain of SdpI is depicted in *blue* and the SBM of the GlyRβ loop sequence in *green*, respectively; corresponding side chains are labeled likewise. Important electrostatic interactions are formed by Lys-434 of GlyRβ with Glu-417 of SdpI, and by Lys-435 with residues Gln-396, Glu-397, and Glu-400, respectively. In addition, there is a Pro-441 to Asn-436 backbone carbonyl interaction. Pro-438 of GlyRβ is bound in a hydrophobic environment generated by residues Trp-420, Pro-434, and Tyr-437 of SdpI, whereas Pro-441 interacts with tyrosines Tyr-391 and Tyr-437. In the *left panel*, the N and C termini of the GlyRβ SBM are located on the *left* and *right*, respectively, and the *right panel* shows the SH3 domain/SBM complex rotated by 180°.

crystal structures. A three-dimensional structure of SdpI has been solved more recently (42). However, in this structure the SH3 domain interacts with two right-handed α-helices of the F-BAR domain, whereas molecular dynamics simulations predict the SBM of GlyRβ to contain a left-handed polyproline type II helix (Fig. 3*C*) (40). Furthermore, the SH3 domain binding sequences of the F-BAR domain and GlyRβ exhibit only very low homology. We therefore searched for optimal fits in the database and selected the x-ray structures 2DRM (SH3 domain displaying 63% similarity and 49% identity with SdpI in complex with a left-handed polyproline type II helix) and 1RLQ (polyproline type II helix in the correct binding orientation with a binding motif most similar to GlyRβ (R*XX*P*XX*P) in complex with an SH3 domain) as templates for homology modeling of the SH3 domain of SdpI and the GlyRβ SBM, respectively. The resulting energy-minimized model of the SdpI-SH3·GlyRβ complex is shown in Fig. 3*C*. The central residue Pro-438 of the GlyRβ SBM (included in the PPAA double substitution) is embedded in a hydrophobic pocket of the SH3 domain of SdpI formed by residues Trp-420, Pro-434, and Tyr-437 (for P434L

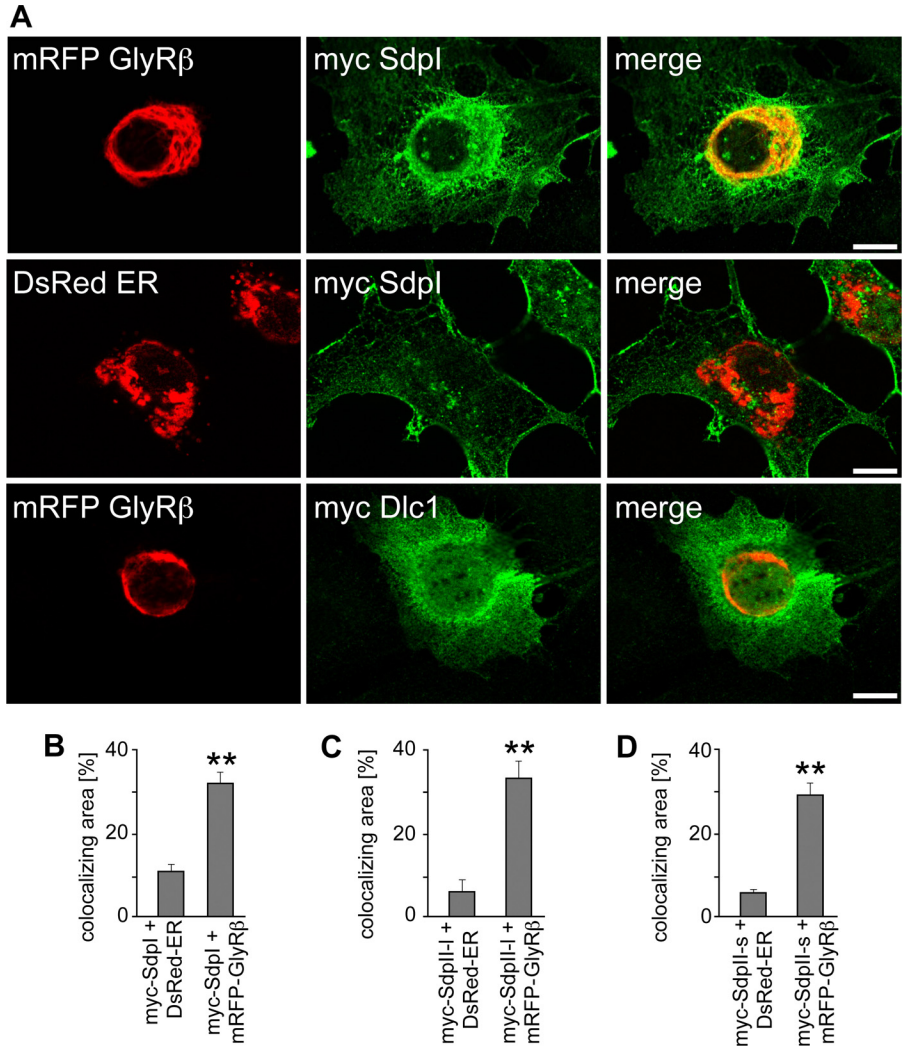

FIGURE 4. **Co-localization of SdpI and SdpII with GlyRβ upon coexpression in COS-7 cells.** *A, top row,* Myc-SdpI was coexpressed with mRFP-GlyRβ. mRFP-GlyRβ was retained in the ER (*red channel*), and Myc-SdpI (*green channel*) partially colocalized with mRFP-GlyRβ (see *right panel*, *yellow signal*). Upon coexpression of Myc-SdpI with DsRed-ER, an ER marker (*middle row*), and of Myc-Dlc1 with mRFP-GlyRβ (*bottom row*), much less colocalization was observed. *Scale bar,* 10 μm. *B,* quantification of Myc-SdpI and mRFP-GlyRβ colocalization. The areas of mRFP-GlyRβ or DsRed-ER colocalizing with the Myc-tagged SdpI protein were determined. Note that colocalization of Myc-SdpI with mRFP-GlyRβ was significantly higher than with DsRed-ER. *C* and *D,* quantifications obtained from corresponding coexpression experiments with Myc-SdpII-l (*C*) and Myc-SdpII-s (*D*). Both SdpII splice variants displayed significant colocalization with mRFP-GlyRβ but not DsRed-ER. **, $p \leq 0.01$. Data represent means ± S.E. from three independent experiments with $n = 200$ (SdpII-s, $n = 300$) cells per assay.

mutation, see Fig. 2, *A* and *B*). The residues Lys-434 and Lys-435 exchanged in the KKAA mutant are involved in electrostatic interactions, *i.e.* Lys-435 of GlyRβ with Gln-396, Glu-397, and Glu-400 of SdpI, and Lys-434 with Glu-417. Furthermore, Pro-441 in the C-terminal end of the SBM interacts via its carbonyl backbone with Asn-436, and with tyrosines 391 and 437. In summary, the model shown in Fig. 3*C* supports our biochemical results.

GlyRβ and Sdps Colocalize in Mammalian Cells—The results presented above show that Sdps and GlyRβ interact *in vitro*. To demonstrate that this interaction also occurs in mammalian cells, we coexpressed these proteins in COS-7 cells. In the absence of GlyRα subunits, GlyRβ is known to be retained in the ER (6). Based on this observation, we used an ER retention assay for monitoring Sdp interactions with GlyRβ. First, we confirmed the validity of this assay by coexpressing mRFP-GlyRβ in COS-7 cells together with GFP-gephyrin. In agreement with earlier observations (6), this resulted in a significant colocalization of both proteins in the ER, whereas a previously described gephyrin mutant unable to interact with GlyRβ (23) formed aggregates in the cytosol (data not shown). Upon coexpression of Myc-tagged SdpI with mRFP-GlyRβ, Myc-SdpI was found to colocalize with mRFP-GlyRβ to a much higher extent (32.3 ± 2.8% area colocalizing) than obtained upon coexpression of Myc-SdpI with a vector staining the ER (DsRed ER; 11.4 ± 1.7%, $p < 0.01$; Fig. 4*B*) or compared with the colocalization of Dlc1, a Myc-tagged gephyrin-binding protein (7), with mRFP-GlyRβ (9.5 ± 3.8%, $p < 0.05$) (Fig. 4, *A* and *B*, and data not shown). Similarly, significant colocalization with mRFP-GlyRβ was observed for both SdpII-l (33.5 ± 4.3% *versus* 6.2 ± 2.9% for SdpII-l with DsRed ER, $p < 0.01$; Fig. 4*C*) and SdpII-s (29.2 ± 2.9% as compared with 6.0 ± 0.8% for SdpII-s with DsRed ER; Fig. 4*D*). These results demonstrate that Sdps can interact with GlyRβ in mammalian cells.

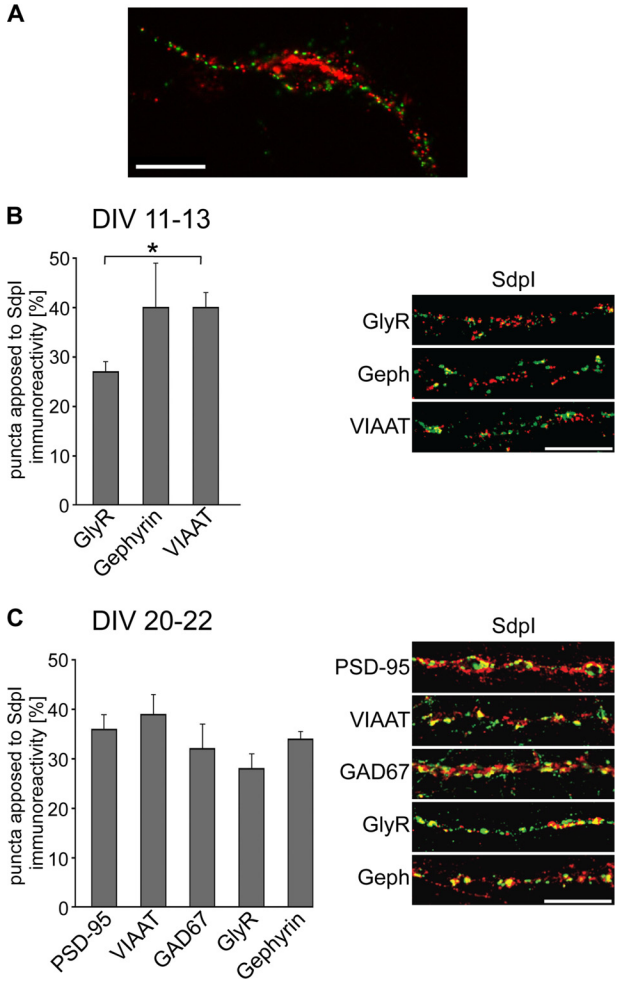

FIGURE 5. **Synaptic localization of SdpI in rat spinal cord neurons.** *A*, spinal cord neurons were stained for SdpI (*red*) and gephyrin (*green*) at DIV13. Intense SdpI staining is seen ubiquitously in the soma and enriched at some locations near the plasma membrane. In addition, SdpI immunoreactive puncta are found along neuronal processes, often apposed to gephyrin clusters. *B, right panel,* spinal cord neurons were stained for SdpI (*red*) and GlyR (*top row, green*), gephyrin (*middle row, green*), and VIAAT (*bottom row, green*) at DIV11–13. *Left panel,* quantification of the colocalizations shown exemplarily in the *right panel*. The colocalization of VIAAT with SdpI was significantly higher than that with the GlyR. *, $p \leq 0.05$. *C,* spinal cord neurons analyzed at a later stage (DIV20–22) and for even more synaptic marker proteins. Again, SdpI (*red*) exhibited clear appositions to VIAAT (*green*), gephyrin (*green*), and GlyR (*green*) immunoreactive puncta. In addition, comparable fractions of the structures positive for GAD67 (*green*), a presynaptic marker for GABAergic terminals, and PSD-95 (*green*), a postsynaptic protein of excitatory synapses, were apposed to SdpI. Data represent means ± S.E. from three independent experiments with $n = 10$ neurons per condition assay. *Scale bars,* 10 μm.

Synaptic Localization of SdpI in Cultured Rat Spinal Cord Neurons—A prerequisite for a physiological role of SdpI binding to GlyRβ is the colocalization of both proteins in neurons. Initial Western blot experiments had revealed that SdpI is expressed not only in brain but also in spinal cord, where GlyRs are abundant (data not shown). We hence double-immunostained cultured embryonic rat spinal cord neurons at DIV11–13, *i.e.* a time point when many glycinergic synapses are known to be formed (43), with antibodies specific for SdpI and different synaptic marker proteins. This revealed punctate SdpI immunoreactivity in the soma and along the dendrites (Fig. 5*A*). A considerable fraction of the dendritic SdpI puncta colocalized or overlapped with glycinergic postsynapses (27 ± 2%; Fig. 5*B*), as identified by immunostaining with a GlyR-specific monoclonal antibody. Notably, the fraction of SdpI puncta apposed to VIAAT immunoreactive puncta, *i.e.* inhibitory nerve terminals visualized by an antibody specific for this synaptic vesicle protein ("VIAAT boutons"), was even higher (40 ± 3%, $p \leq 0.05$) and identical to the extent of colocalization found with gephyrin clusters (40 ± 9%, $p > 0.05$). This suggests that SdpI is found not only at glycinergic but also at GABAergic and mixed glycinergic/GABAergic (44) synapses. To unravel whether the occurrence of numerous nonapposed SdpI puncta in these stainings might reflect the presence of SdpI at excitatory synapses, we repeated these double-immunolabeling experiments at a later developmental stage (DIV20–22) and for a larger number of marker proteins (Fig. 5*C*). This confirmed the partial colocalization of SdpI punctate staining with GlyR (28 ± 3%), gephyrin (34 ± 2%), and VIAAT (39 ± 4%) immunoreactivities. Additionally, we found appositions to other established markers of inhibitory and excitatory synapses, *e.g.* the 67-kDa isoform of the GABA-synthesizing enzyme, GAD67, that stains presynaptic inhibitory terminals (32 ± 5%) and the postsynaptic scaffolding protein PSD-95 localized in the postsynaptic densities of excitatory synapses (36 ± 3%). These results are consistent with SdpI being present at glycinergic, GABAergic, and glutamatergic synapses.

SdpI Knockdown Reduces GlyR Cluster Density and Size in Cultured Spinal Neurons—The results described above indicated that in spinal cord neurons SdpI is present at a significant fraction of GlyR-containing inhibitory synapses. To determine whether SdpI might contribute to GlyR synaptic trafficking and/or localization, we performed acute SdpI knockdown experiments in cultured spinal cord neurons using a vector-based microRNA-adapted short hairpin approach. The recombinant adeno-associated virus system (45) was employed for efficient delivery of the knockdown vectors at DIV7. Western blotting at DIV20 showed that infection with the SdpI-miR virus reduced SdpI expression to 39 ± 16% of the level found in sister cultures infected with a control-miR virus (Fig. 6, *A* and *B*). This down-regulation could be overcome by a siRNA-resistant Myc-tagged SdpI construct (SdpI-siR), which produced strong SdpI overexpression when coinfected with the SdpI-miR virus (812 ± 469% of control) but also cell death due to viral overload, as indicated by a major loss of anti-β3-tubulin (Fig. 6*A*).

Using the SdpI-miR knockdown conditions described above, we found clear reductions in the density (clusters/50-μm neurite length, 17 ± 3 in SdpI-miR *versus* 35 ± 5 in control-miR-infected neurons, $p \leq 0.05$) and average size (0.25 ± 0.01 μm^2 in SdpI-miR *versus* 0.32 ± 0.01 μm^2 in control-miR-infected cultures, $p \leq 0.05$) of GlyR clusters upon infection with SdpI-miR (Fig. 6, *C–E*). Co-infection with the siRNA resistant SdpI construct rescued both effects (GlyR cluster density 38 ± 1 puncta/50-μm neurite length and mean size 0.39 ± 0.02 μm^2, both $p \leq 0.01$ as compared with SdpI-miR-infected sister cultures; Fig. 6, *C–E*).

To examine whether the viral SdpI-miR knockdown specifically affects GlyRs, we also performed SdpI knockdown experiments, in which other marker proteins of inhibitory synapses were analyzed. However, in contrast to the changes in GlyR

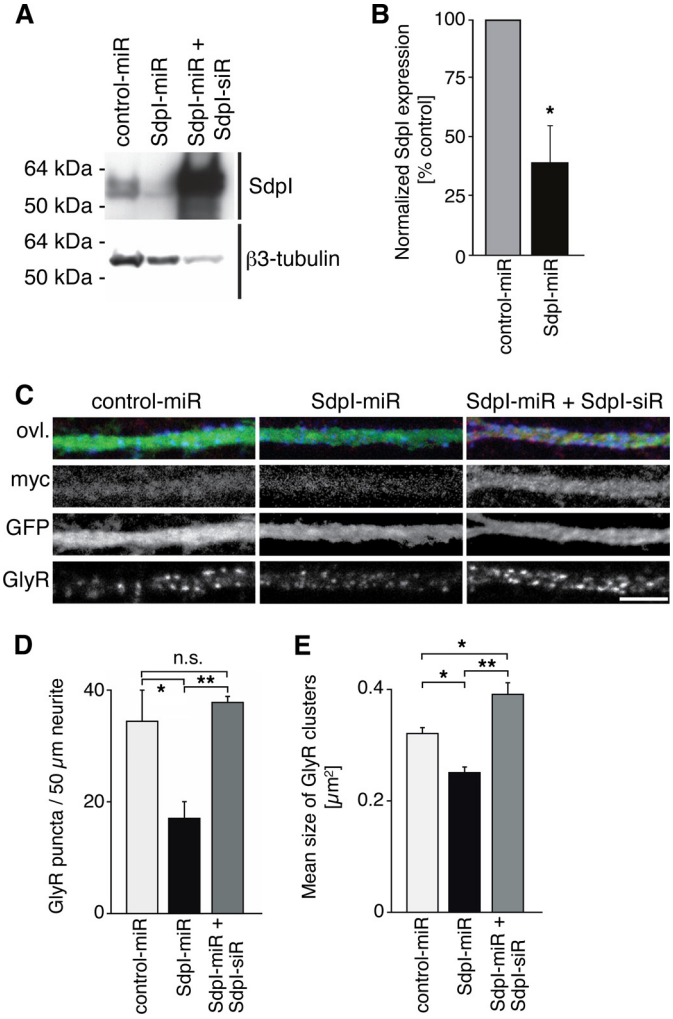

FIGURE 6. **SdpI knockdown in rat spinal cord neurons.** *A,* Western blot showing β3-tubulin and SdpI expression in spinal cord neurons infected with control-miR, SdpI-miR, and coinfected with SdpI-miR and SdpI-siR, the latter additionally providing a Myc tag for SdpI. *B,* summary *bar graph* showing the efficiency of SdpI knockdown in spinal cord neurons normalized to β3-tubulin. Knockdown by RNA interference during 14 days significantly reduced SdpI expression, *, $p \leq 0.05$. *C,* immunostainings demonstrating reduced mean GlyR cluster size and density in SdpI knockdown neurons. The following epitopes were detected: *Myc*, staining of Myc-tagged SdpI-siR with anti-Myc antibody; *GFP,* reporter expression in all three panels indicated that the neurons were successfully infected; *GlyR*, SdpI-miR knockdown (*middle panel*) resulted in reduced staining as compared with control-miR infected cells (*left panel*), but immunoreactivity was restored upon coinfection of SdpI-siR (*right panel*). *Top row,* overlay (*ovl.*) of the fluorescence signals (*red,* Myc; *green,* GFP; *blue,* GlyR). *Scale bar,* 5 μm. *D* and *E,* quantification of experiments as shown in *C*. Note significant reduction of both GlyR cluster density (*D*) and size (*E*) in SdpI-miR infected cells (both *, $p \leq 0.05$). Co-expression of SdpI-siR rescued both parameters (**, $p \leq 0.01$). *n.s.,* not significant. Data represent means ± S.E. from three independent experiments with $n = 10$ neurons per condition assay.

cluster properties observed upon SdpI-miR infection, neither significant reductions in the relative densities of gephyrin clusters (89 ± 18% of control; $p > 0.05$) and VIAAT immunoreactive boutons (97 ± 14% of control; $p > 0.05$) nor in their average sizes (73 ± 21% of control for gephyrin clusters; 74 ± 13% of control for VIAAT boutons; both $p > 0.05$) were found (data not shown). Thus, SdpI deficiency appears to specifically affect GlyR cluster properties. Notably, SDS-PAGE followed by immunoblotting with mAb4a failed to reveal reductions in GlyRα protein levels in the SdpI-miR-infected cultures (data not shown). Hence, the reduced density and size of GlyR clusters observed upon SdpI knockdown are not due to enhanced receptor degradation.

GlyR Cluster Sizes and Densities In Brainstem Sections and Cultured Neurons Derived from SdpI$^{-/-}$ Mice—To further corroborate a role of SdpI in synaptic GlyR trafficking and/or localization, we analyzed the densities and sizes of GlyR clusters and VIAAT boutons in brainstem sections prepared from adult SdpI$^{-/-}$ and WT littermates. However, no significant differences between genotypes could be detected (GlyR clusters/10,000 μm^2, 738 ± 128 in WT *versus* 609 ± 57 in SdpI$^{-/-}$; GlyR cluster size, 0.355 ± 0.019 μm^2 in WT *versus* 0.320 ± 0.021 μm^2 in SdpI$^{-/-}$; VIAAT boutons/10,000 μm^2, 851 ± 39 in WT *versus* 727 ± 89 in SdpI$^{-/-}$; VIAAT bouton size, 0.520 ± 0.053 μm^2 in WT *versus* 0.509 ± 0.027 μm^2 in SdpI$^{-/-}$; all $p > 0.05$; see Fig. 7, *A* and *B*). This could not be attributed to an up-regulation of any of the other less abundant Sdp isoforms, SdpII and SdpIII, in the mutant animals. A semi-quantitative analysis of immunoblots of brainstem detergent extracts prepared from adult SdpI$^{-/-}$ ($n = 5$) and WT ($n = 6$) animals revealed relative expression levels (normalized to actin) of 96 ± 8% for SdpII and of 97 ± 8% for SdpIII, as compared with WT (data not shown).

Because GlyRs accumulate at inhibitory synapses primarily during early developmental stages, we examined GlyR cluster formation in spinal cord cultures prepared from SdpI$^{-/-}$ mice (20) at embryonic day 14.5. After 21 days of *in vitro* differentiation (43), the average size of GlyR clusters was found to be significantly lower in SdpI$^{-/-}$ neurons as compared with that in WT cells (0.340 ± 0.021 μm^2 in WT *versus* 0.240 ± 0.018 μm^2 in SdpI$^{-/-}$; $p \leq 0.05$; see Fig. 7, *C* and *D*). Furthermore, the average number of GlyR clusters per 50-μm dendrite was lower in SdpI$^{-/-}$ as compared with WT neurites (32 ± 1 in WT *versus* 24 ± 2 in SdpI$^{-/-}$; $p \leq 0.05$). In contrast to these alterations seen for synaptic GlyRs, no significant differences were observed in the average sizes of both postsynaptic gephyrin clusters (0.537 ± 0.025 μm^2 in WT *versus* 0.518 ± 0.017 μm^2 in SdpI$^{-/-}$) and VIAAT-positive presynaptic terminals (0.450 ± 0.018 μm^2 in WT *versus* 0.431 ± 0.069 μm^2 in SdpI$^{-/-}$) and their corresponding densities (29 ± 1 per 50-μm dendrite in WT *versus* 31 ± 1 in SdpI$^{-/-}$ for gephyrin clusters; and 27 ± 3 in WT *versus* 27 ± 5 in SdpI$^{-/-}$ for VIAAT boutons; both $p > 0.05$) (Fig. 7, *C* and *D*). Together, the results obtained from the SdpI$^{-/-}$ brainstem sections and cultured spinal neurons are consistent with SdpI contributing primarily to the formation of synaptic GlyR clusters at early stages of neuronal differentiation and synaptogenesis.

DISCUSSION

In this study, we identified SdpI by affinity binding and MS as a novel binding protein of GlyRβ. SdpI coimmunoprecipitates with native GlyR from brainstem detergent extracts. Using deletion approaches and point mutation analysis, SdpI binding to GlyRβ was found to be mediated by a classical SH3 domain-ligand interaction and thus defines the first intracellular protein binding to the previously predicted SBMs of GlyRs (1). Upon coexpression in COS-7 cells, SdpI and both splice variants of SdpII colocalized with GlyRβ. In cultured spinal cord neurons containing reduced levels of or lacking SdpI, the mean sizes and

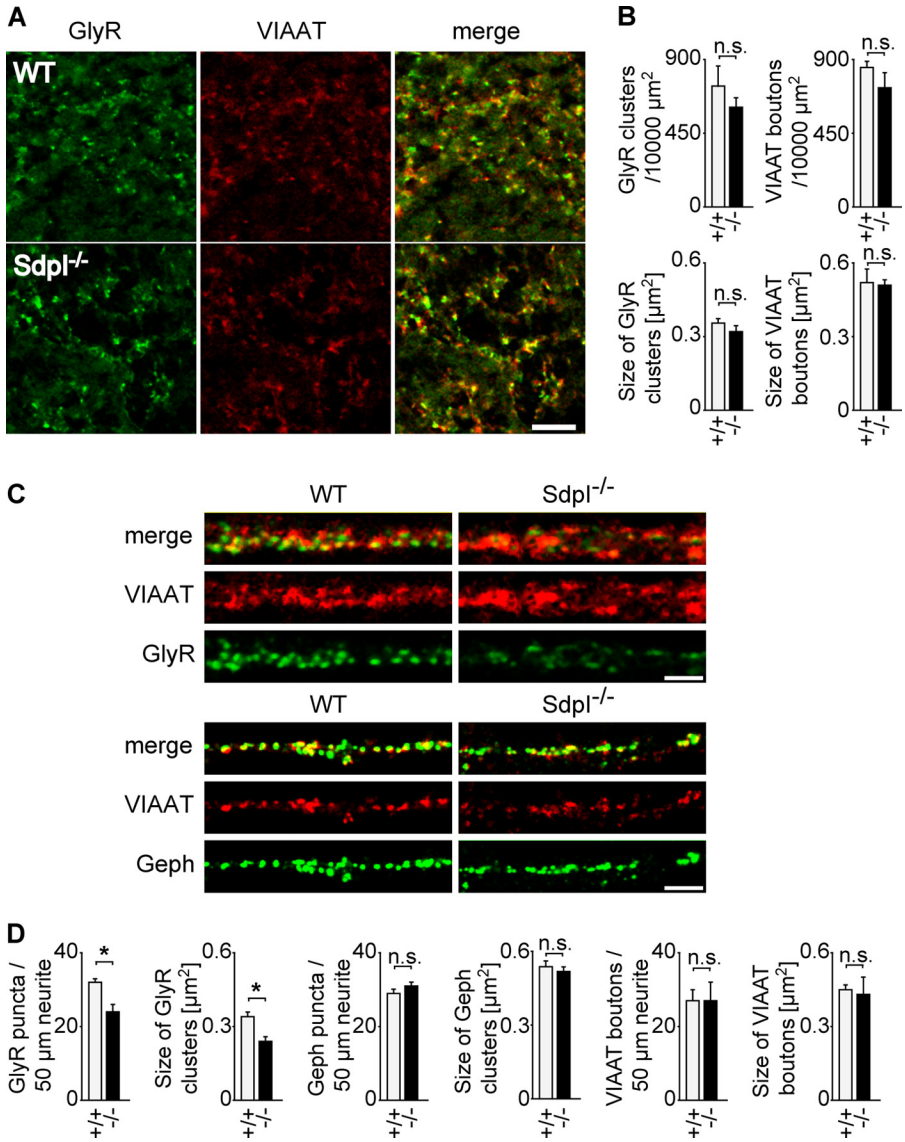

FIGURE 7. **GlyR clusters in adult brainstem and cultured spinal cord neurons from Sdpl$^{-/-}$ mice.** *A,* immunostainings for GlyR (*green*) and VIAAT (*red*) in brainstem sections from adult WT and Sdpl$^{-/-}$ mice. GlyR and VIAAT cluster densities and sizes appeared comparable in Sdpl$^{-/-}$ and WT brainstems. *Scale bar,* 10 μm. *B,* quantification of experiments as shown in *A*. No significant differences in GlyR cluster and VIAAT bouton densities and sizes were found between WT and Sdpl$^{-/-}$ sections (all $p > 0.05$; data represent means ± S.E. from three animals analyzed per genotype). *C,* immunostainings showing reduced mean GlyR cluster size and density in Sdpl$^{-/-}$ spinal cord neurons. Spinal cord neurons were prepared from WT or Sdpl$^{-/-}$ mouse embryos and stained at DIV21 for GlyR (*green channel* in *upper panels*), VIAAT (*red channel* in *upper* and *lower panels*), and gephyrin (*green channel* in *lower panels*). *Scale bars,* 5 μm. *D,* quantifications of densities and sizes of GlyR and gephyrin clusters and of VIAAT boutons, determined from immunostained neurons as shown in *C*. Note significant reductions in GlyR cluster density and size in Sdpl$^{-/-}$ as compared with WT spinal neurons (*, $p \leq 0.05$). In contrast, gephyrin cluster and VIAAT bouton densities and sizes were not significantly different between genotypes (all $p > 0.05$; 20 cells each analyzed per genotype in three independent experiments). *n.s.,* not significant.

densities of postsynaptic GlyR clusters were decreased, whereas in adult mice SdpI deficiency did not affect GlyR clusters. Our results are consistent with a function of SdpI in the trafficking and/or cytoskeletal anchoring of synaptic GlyRs that is redundant at adult stages.

Molecular Basis of Sdp Binding to GlyRβ—The SH3 domains are highly conserved between SdpI, SdpII, and SdpIII (15, 46). This explains why we observed binding not only of SdpI but also of SdpII to GlyRβ and suggests that SdpIII may also interact with GlyRβ.

The binding region of GlyRβ contains a KK*XXP*XXP motif. The proline residues of this motif are likely to form a left-handed polyproline type II helix, whereas its lysine residues are thought to provide binding specificity by electrostatically interacting with residues of the SH3 domain (40). Indeed, our modeling suggests that lysine 435 interacts with glutamate residues 397 and 400 of the SH3 domain of SdpI; this might help to orient the ligand motif within the binding groove of the SH3 domain (40). The KK*XXP*XXP motif is highly conserved and found not only in rat and human but also in chick, fish, and frog GlyRβ sequences. This conservation underlines its importance and suggests that the interaction of Sdps with GlyRβ occurs in all vertebrates.

Polyproline type II helices provide the structural scaffold for SBM-SH3 domain interactions. Molecular dynamics simulations suggested that, similar to the corresponding proline of the template structure 1RLQ (47), Pro-441 of GlyRβ is directly involved in interactions with the SH3 domain. However, only

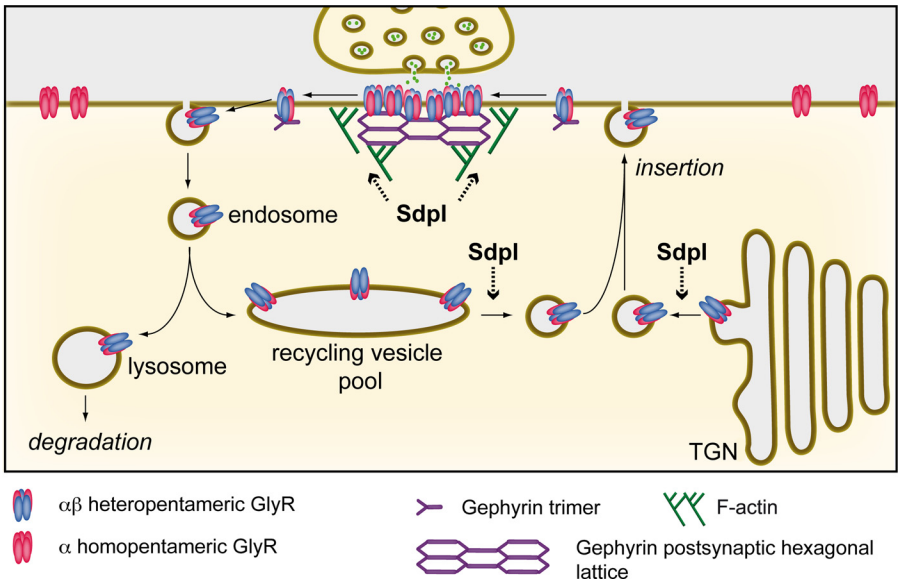

FIGURE 8. **Model for possible roles of SdpI in the intracellular trafficking and cytoskeletal anchoring of synaptic GlyRs.** After synthesis, GlyRs are transported via the trans-Golgi network (*TGN*) to the plasma membrane and from there as receptor·gephyrin complexes to inhibitory postsynaptic sites, where gephyrin assembles into a hexagonal scaffold that is stabilized by interactions with the actin cytoskeleton. GlyRs may dissociate from postsynaptic sites with or without bound gephyrin and either be re-immobilized at other postsynapses or endocytosed. Following endocytosis, GlyRs can be recycled or degraded. SdpI might be involved in GlyR transport from the trans-Golgi network to the plasma membrane (*right*), in GlyR recycling (*center*), or in regulating the subsynaptic (or perisynaptic cortical) actin cytoskeleton (*center top*).

minor effects were seen upon its deletion or point mutation; this likely reflects an only partial contribution of Pro-441 to SdpI binding in addition to the side chain interactions mediated by Pro-438 and lysines Lys-434 and Lys-435. Notably, the binding of SdpI to the GTPase dynamin depends on a similar motif, RR*X*P*XX*P, in which arginine residues provide positive charges for SdpI association (18). Recently, K*X*RAP*X*PP motifs have been implicated in SdpI binding to the actin nucleator cordon bleu (48). A comparison of all these SdpI-binding motifs reveals that dynamin and GlyRβ and two of the three cordon bleu-binding sites all share the well known motif (R/K)*XX*P*XX*P involved in SH3 domain binding of polyproline type II helices (40).

It is noteworthy that the SBM of GlyRβ as identified here (residues 427–448) is distinct from, but located adjacent to, the other known intracellular protein binding regions, *i.e.* the GBM and the Vps35 and Nbea interaction sites, which all lie within GlyRβ(378–426) (5, 6, 10). Thus, SdpI and these other proteins might bind simultaneously to a single GlyRβ subunit. This may be of physiological relevance, as GlyRs are known to interact with gephyrin not only at synapses but also at different stages of intracellular transport (8, 9). Moreover, pentameric synaptic GlyRs are thought to contain three copies of GlyRβ (4). Hence, simultaneous binding of different interacting proteins by a single pentameric GlyR may occur at variable stoichiometries.

Localization of SdpI in Spinal Cord Neurons—So far, SdpI has been studied pre- and postsynaptically at excitatory synapses in rat hippocampus (24, 48, 49) and presynaptically at the reticulospinal synapse in lamprey (19). Additionally, SdpI has been found in parvalbumin-positive inhibitory interneurons of the mouse brain (20). Here, we confirmed the presence of SdpI at excitatory synapses, as revealed by apposition to PSD-95 (Fig. 5*C*). Additionally we found SdpI immunoreactivity at inhibitory synapses as indicated by its vicinity to GlyR clusters (Fig. 5*B*). Notably, at DIV11–13 colocalization with VIAAT boutons was significantly higher than with GlyR clusters (Fig. 5*B*). This finding suggested that SdpI is present not only at glycinergic but also at other inhibitory synapses. Indeed, at DIV20–22 we saw colocalization of SdpI with GAD67, the presynaptically localized GABA-synthesizing enzyme, to a similar extent as compared with VIAAT, gephyrin, and the GlyR (Fig. 5*C*). Our results are consistent with SdpI being present at glutamatergic, glycinergic, and GABAergic synapses of spinal cord neurons.

Putative Functions of SdpI in the Trafficking and Cytoskeletal Anchoring of Synaptic GlyRs—Sdps have been implicated in vesicle formation at the plasma membrane and the trans-Golgi network and in endocytotic receptor recycling (15–20). Additionally, SdpI has been reported to mediate endocytotic removal of NR3A containing *N*-methyl-D-aspartate (NMDA) receptors from excitatory postsynapses (49). These reports are consistent with SdpI regulating dynamin-driven fission of endocytotic and transport vesicles from their donor membranes (15, 17, 18, 20). In this study, we observed decreases in GlyR cluster size and density upon SdpI knockdown or gene inactivation in cultured neurons, whereas GlyR expression levels as detected by immunoblotting were unchanged under knockdown conditions. Our results are difficult to reconcile with a function of SdpI in GlyR internalization or degradation but are consistent with its contribution to the formation of GlyR containing transport vesicles or other membrane fission-dependent trafficking steps occurring after the assembly of the receptor pentamer required for GlyR exit from the ER (50). As schematically depicted in Fig. 8, *right*, SdpI might contribute to the budding of GlyR transport vesicles from the Golgi apparatus. Alternatively, local recycling mechanisms for synaptic GlyRs might exist in dendrites which, in analogy to the synaptic re-insertion of excitatory 2-amino-3-(3-hydroxy-5-methylisoxazol-4-yl)propanoic acid (AMPA) receptors from an intracellular pool localized in dendritic spines (51), allow for the

adjustment of synaptic strength of individual inhibitory synapses to changes in neuronal activity (Fig. 8, *center*). Such receptor recycling processes are likely to involve an endosome-derived recycling vesicle pool, from which GlyR containing vesicles are generated for re-incorporation into the plasma membrane in a SdpI-dependent membrane fission reaction. Consistent with this proposal, previous reports have shown that SdpI is required for synaptic vesicle recycling in presynaptic nerve terminals (19, 20).

In addition to eliminating functions of SdpI in the intracellular trafficking and/or recycling of GlyRs as proposed above, SdpI deficiency may directly affect the organization or stability of GlyR clusters at inhibitory postsynapses. Previous studies have shown that the pharmacological disruption of the actin cytoskeleton leads to a loss of gephyrin and GlyRs from synaptic sites (52, 53). Moreover, the actin regulatory proteins profilin and ena/VASP interact with gephyrin and have been implicated in the regulation of synaptic GlyR densities by microfilaments (39, 54, 55). SdpI is known to bind the Arp2/3 complex activator neural Wiskott-Aldrich syndrome protein (N-WASP), thereby releasing N-WASP's auto-inhibition and thus enhancing actin polymerization (32). Consequently, SdpI knockdown or deficiency should reduce N-WASP activity and thereby result in a weakening of the local F-actin meshworks present at postsynaptic sites, which in turn should decrease GlyR cluster density and/or size (see Fig. 8, *center top*). This local destabilization of synaptic F-actin might be further enhanced by additional effects of reduced SdpI levels on the actin nucleator cordon bleu (48). In conclusion, SdpI could contribute to synaptic GlyR anchoring by regulating receptor immobilization via the actin cytoskeleton. It should, however, be noted that we found no significant change in gephyrin cluster properties in our SdpI loss-of-function experiments. This suggests that the consequences of SdpI deficiency are gephyrin-independent and thus likely to not target GlyRs already localized at synapses. In agreement with this view, previous analyses of gephyrin-deficient mice have shown that gephyrin is not required for the insertion of GlyRs and the related $GABA_A$ receptors into the neuronal plasma membrane (56, 57). We therefore propose that binding of SdpI to GlyRβ primarily regulates the intracellular trafficking of synaptic GlyRs.

A puzzling finding of this study is the lack of detectable changes in GlyR cluster number and size in brainstem sections derived from adult $SdpI^{-/-}$ mice. This result could reflect limitations in the sensitivity of our immunostaining procedure, but it might also be due to a compensation of the SdpI deficiency by either of the less abundant SdpI isoforms, *e.g.* SdpII and SdpIII, or by other functionally related trafficking proteins that are expressed only at later developmental stages. Here, immunoblotting experiments confirmed the expression of SdpII and SdpIII in brainstem but failed to reveal an up-regulation of these proteins in $SdpI^{-/-}$ mice, which are known to suffer from impaired inhibitory neurotransmission (20). Clearly, a more detailed investigation of the consequences of SdpI deficiency on the formation and function of glycinergic synapses is warranted.

The GlyRβ Loop, a Key Determinant of Synaptic GlyR Trafficking and Immobilization—The cytoplasmic loop of GlyRβ is known to be essential for the synaptic localization of GlyRs due to its tight interaction with gephyrin (5, 6), and immunostainings with a monoclonal antibody specific for this GlyR subunit have confirmed its presence at the vast majority of glycinergic synapses in the rodent central nervous system (58). Recently, we identified the trafficking proteins Vps35 and Nbea as additional interaction partners of the GlyRβ loop (10). Here, we further extend the number of GlyRβ-binding proteins by adding SdpI, which interacts via its SH3 domain. The underlying SH3 domain-SBM interaction appears to be of high affinity, because our proteomic search employed stringent biochemical conditions to select for robust interactions. Hence, less abundant proteins may have escaped detection, a view that is supported by the observation that only SdpI but not SdpII, which is also expressed in brain (14) and clearly binds GlyRβ, was consistently detected by MS in our pulldown experiments. Thus, additional binding partners of GlyRβ might exist that remain to be identified. The SBMs of GlyRs have been recognized some time ago (1); our results provide a first indication for a role of these motifs in GlyR regulation.

Acknowledgments—We thank Drs. Matthias Kneussel, Sebastian Kügler, and Jürgen Kleinschmidt for kindly providing constructs; Dr. Rolf Sprengel for help with the AAV system; Dr. Bertram Schmitt for many helpful discussions and support, and Helene Geptin for expert technical assistance.

REFERENCES

1. Lynch, J. W. (2004) Molecular structure and function of the glycine receptor chloride channel. *Physiol. Rev.* **84,** 1051–1095
2. Grenningloh, G., Rienitz, A., Schmitt, B., Methfessel, C., Zensen, M., Beyreuther, K., Gundelfinger, E. D., and Betz, H. (1987) The strychnine-binding subunit of the glycine receptor shows homology with nicotinic acetylcholine receptors. *Nature* **328,** 215–220
3. Grenningloh, G., Pribilla, I., Prior, P., Multhaup, G., Beyreuther, K., Taleb, O., and Betz, H. (1990) Cloning and expression of the 58 kd β subunit of the inhibitory glycine receptor. *Neuron* **4,** 963–970
4. Grudzinska, J., Schemm, R., Haeger, S., Nicke, A., Schmalzing, G., Betz, H., and Laube, B. (2005) The β subunit determines the ligand binding properties of synaptic glycine receptors. *Neuron* **45,** 727–739
5. Kneussel, M., Hermann, A., Kirsch J., and Betz, H. (1999) Hydrophobic interactions mediate binding of the glycine receptor β-subunit to gephyrin. *J. Neurochem.* **72,** 1323–1326
6. Meyer, G., Kirsch, J., Betz, H., and Langosch, D. (1995) Identification of a gephyrin-binding motif on the glycine receptor β subunit. *Neuron* **15,** 563–572
7. Fuhrmann, J. C., Kins, S., Rostaing, P., El Far, O., Kirsch, J., Sheng, M., Triller, A., Betz, H., and Kneussel, M. (2002) Gephyrin interacts with Dynein light chains 1 and 2, components of motor protein complexes. *J. Neurosci.* **22,** 5393–5402
8. Maas, C., Tagnaouti, N., Loebrich, S., Behrend, B., Lappe-Siefke, C., and Kneussel, M. (2006) Neuronal cotransport of glycine receptor and the scaffold protein gephyrin. *J. Cell Biol.* **172,** 441–451
9. Maas, C., Belgardt, D., Lee, H.K., Heisler, F. F., Lappe-Siefke, C., Magiera, M. M., van Dijk, J., Hausrat, T. J., Janke, C., and Kneussel, M. (2009) Synaptic activation modifies microtubules underlying transport of postsynaptic cargo. *Proc. Natl. Acad. Sci. U.S.A.* **106,** 8731–8736
10. del Pino, I., Paarmann, I., Karas, M., Kilimann, M. W., and Betz, H. (2011) The trafficking proteins vacuolar protein sorting 35 and neurobeachin interact with the glycine receptor β-subunit. *Biochem. Biophys. Res. Commun.* **412,** 435–440
11. Qualmann, B., and Kessels, M. M. (2002) Endocytosis and the cytoskeleton. *Int. Rev. Cytol.* **220,** 93–144
12. Itoh, T., Erdmann, K. S., Roux, A., Habermann, B., Werner, H., and De

Camilli, P. (2005) Dynamin and the actin cytoskeleton cooperatively regulate plasma membrane invagination by BAR and F-BAR proteins. *Dev. Cell* **9,** 791–804
13. Qualmann, B., Koch, D., and Kessels, M. M. (2011) Let's go bananas: revisiting the endocytic BAR code. *EMBO J.* **30,** 3501–3515
14. Kessels, M. M., and Qualmann, B. (2004) The syndapin protein family: linking membrane trafficking with the cytoskeleton. *J. Cell Sci.* **117,** 3077–3086
15. Qualmann, B., and Kelly, R. B. (2000) Syndapin isoforms participate in receptor-mediated endocytosis and actin organization. *J. Cell Biol.* **148,** 1047–1062
16. Braun, A., Pinyol, R., Dahlhaus, R., Koch, D., Fonarev, P., Grant, B.D., Kessels, M. M., and Qualmann, B. (2005) EHD proteins associate with syndapin I and II and such interactions play a crucial role in endosomal recycling. *Mol. Biol. Cell* **16,** 3642–3658
17. Kessels, M. M., Dong, J., Leibig, W., Westermann, P., and Qualmann, B. (2006) Complexes of syndapin II with dynamin II promote vesicle formation at the trans-Golgi network. *J. Cell Sci.* **119,** 1504–1516
18. Anggono, V., and Robinson, P. J. (2007) Syndapin I and endophilin I bind overlapping proline-rich regions of dynamin I: role in synaptic vesicle endocytosis. *J. Neurochem.* **102,** 931–943
19. Andersson, F., Jakobsson, J., Löw, P., Shupliakov, O., and Brodin, L. (2008) Perturbation of syndapin/PACSIN impairs synaptic vesicle recycling evoked by intense stimulation. *J. Neurosci.* **28,** 3925–3933
20. Koch, D., Spiwoks-Becker, I., Sabanov, V., Sinning, A., Dugladze, T., Stellmacher, A., Ahuja, R., Grimm, J., Schüler, S., Müller, A., Angenstein, F., Ahmed, T., Diesler, A., Moser, M., Tom Dieck, S., Spessert, R., Boeckers, T. M., Fässler, R., Hübner, C. A., Balschun, D., Gloveli, T., Kessels, M. M., and Qualmann, B. (2011) Proper synaptic vesicle formation and neuronal network activity critically rely on syndapin I. *EMBO J.* **30,** 4955–4969
21. Brundiers, R., Lavie, A., Veit, T., Reinstein, J., Schlichting, I., Ostermann, N., Goody, R. S., and Konrad, M. (1999) Modifying human thymidylate kinase to potentiate azidothymidine activation. *J. Biol. Chem.* **274,** 35289–35292
22. Paarmann, I., Lye, M. F., Lavie, A., and Konrad, M. (2008) Structural requirements for calmodulin binding to membrane-associated guanylate kinase homologs. *Protein Sci.* **17,** 1946–1954
23. Sola, M., Bavro, V.N., Timmins, J., Franz, T., Ricard-Blum, S., Schoehn, G., Ruigrok, R. W., Paarmann, I., Saiyed, T., O'Sullivan, G. A., Schmitt, B., Betz, H., and Weissenhorn, W. (2004) Structural basis of dynamic glycine receptor clustering by gephyrin. *EMBO J.* **23,** 2510–2519
24. Qualmann, B., Roos, J., DiGregorio, P. J., and Kelly, R. B. (1999) Syndapin I, a synaptic dynamin-binding protein that associates with the neural Wiskott-Aldrich syndrome protein. *Mol. Biol. Cell* **10,** 501–513
25. Miroux, B., and Walker, J. E. (1996) Over-production of proteins in *Escherichia coli*: mutant hosts that allow synthesis of some membrane proteins and globular proteins at high levels. *J. Mol. Biol.* **260,** 289–298
26. Paarmann, I., Schmitt, B., Meyer, B., Karas, M., and Betz, H. (2006) Mass spectrometric analysis of glycine receptor-associated gephyrin splice variants. *J. Biol. Chem.* **281,** 34918–34925
27. Sali, A., and Blundell, T. L. (1993) Comparative protein modelling by satisfaction of spatial restraints. *J. Mol. Biol.* **234,** 779–815
28. Hess, B., Kutzner, C., van der Spoel, D., and Lindahl, E. (2008) GROMACS 4: algorithms for highly efficient, load-balanced, and scalable molecular simulation. *J. Chem. Theory Comput.* **4,** 435–447
29. Duan, Y., Wu, C., Chowdhury, S., Lee, M. C., Xiong, G., Zhang, W., Yang, R., Cieplak, P., Luo, R., Lee, T., Caldwell, J., Wang, J., and Kollman, P. (2003) A point-charge force field for molecular mechanics simulations of proteins based on condensed-phase quantum mechanical calculations. *J. Comput. Chem.* **24,** 1999–2012
30. Kessels, M. M., and Qualmann, B. (2006) Syndapin oligomers interconnect the machineries for endocytic vesicle formation and actin polymerization. *J. Biol. Chem.* **281,** 13285–13299
31. Shevtsova, Z., Malik, J. M., Michel, U., Bähr, M., and Kügler, S. (2005) Promoters and serotypes: targeting of adeno-associated virus vectors for gene transfer in the rat central nervous system in vitro and in vivo. *Exp. Physiol.* **90,** 53–59
32. Dharmalingam, E., Haeckel, A., Pinyol, R., Schwintzer, L., Koch, D., Kessels, M. M., and Qualmann, B. (2009) F-BAR proteins of the syndapin family shape the plasma membrane and are crucial for neuromorphogenesis. *J. Neurosci.* **29,** 13315–13327
33. Grimm, D., Kern, A., Rittner, K., and Kleinschmidt, J. A. (1998) Novel tools for production and purification of recombinant adenoassociated virus vectors. *Hum. Gene Ther.* **9,** 2745–2760
34. Zolotukhin, S., Byrne, B. J., Mason, E., Zolotukhin, I., Potter, M., Chesnut, K., Summerford, C., Samulski, R. J., and Muzyczka, N. (1999) Recombinant adeno-associated virus purification using novel methods improves infectious titer and yield. *Gene Ther.* **6,** 973–985
35. Gomeza, J., Ohno, K., Hülsmann, S., Armsen, W., Eulenburg, V., Richter, D. W., Laube, B., and Betz, H. (2003) Deletion of the mouse glycine transporter 2 results in a hyperkeplexia phenotype and postnatal lethality. *Neuron* **40,** 797–806
36. Reddy-Alla, S., Schmitt, B., Birkenfeld, J., Eulenburg, V., Dutertre, S., Böhringer, C., Götz, M., Betz, H., and Papadopoulos, T. (2010) PH-domain-driven targeting of collybistin but not Cdc42 activation is required for synaptic gephyrin clustering. *Eur. J. Neurosci.* **31,** 1173–1184
37. Pfeiffer, F., Simler, R., Grenningloh, G., and Betz, H. (1984) Monoclonal antibodies and peptide mapping reveal structural similarities between the subunits of the glycine receptor of rat spinal cord. *Proc. Natl. Acad. Sci. U.S.A.* **81,** 7224–7227
38. Schröder, S., Hoch, W., Becker, C. M., Grenningloh, G., and Betz, H. (1991) Mapping of antigenic epitopes on the α1 subunit of the inhibitory glycine receptor. *Biochemistry* **30,** 42–47
39. Bausen, M., Fuhrmann, J. C., Betz, H., and O'sullivan, G. A. (2006) The state of the actin cytoskeleton determines its association with gephyrin: role of ena/VASP family members. *Mol. Cell. Neurosci.* **31,** 376–386
40. Li, S. S. (2005) Specificity and versatility of SH3 and other proline-recognition domains: structural basis and implications for cellular signal transduction. *Biochem. J.* **390,** 641–653
41. Puntervoll, P., Linding, R., Gemünd, C., Chabanis-Davidson, S., Mattingsdal, M., Cameron, S., Martin, D. M., Ausiello, G., Brannetti, B., Costantini, A., Ferrè, F., Maselli, V., Via, A., Cesareni, G., Diella, F., Superti-Furga, G., Wyrwicz, L., Ramu, C., McGuigan, C., Gudavalli, R., Letunic, I., Bork, P., Rychlewski, L., Küster, B., Helmer-Citterich, M., Hunter, W. N., Aasland, R., and Gibson, T. J. (2003) ELM server: A new resource for investigating short functional sites in modular eukaryotic proteins. *Nucleic Acids Res.* **31,** 3625–3630
42. Rao, Y., Ma, Q., Vahedi-Faridi, A., Sundborger, A., Pechstein, A., Puchkov, D., Luo, L., Shupliakov, O., Saenger, W., and Haucke, V. (2010) Molecular basis for SH3 domain regulation of F-BAR-mediated membrane deformation. *Proc. Natl. Acad. Sci. U.S.A.* **107,** 8213–8218
43. Lévi, S., Vannier, C., and Triller, A. (1998) Strychnine-sensitive stabilization of postsynaptic glycine receptor clusters. *J. Cell Sci.* **111,** 335–345
44. Dumoulin, A., Lévi, S., Riveau, B., Gasnier, B., and Triller, A. (2000) Formation of mixed glycine and GABAergic synapses in cultured spinal cord neurons. *Eur. J. Neurosci.* **12,** 3883–3892
45. Grimm, D., Kay, M. A., and Kleinschmidt, J. A. (2003) Helper virus-free, optically controllable, and two-plasmid-based production of adeno-associated virus vectors of serotypes 1 to 6. *Mol. Ther.* **7,** 839–850
46. Modregger, J., Ritter, B., Witter, B., Paulsson, M., and Plomann, M. (2000) All three PACSIN isoforms bind to endocytic proteins and inhibit endocytosis. *J. Cell Sci.* **113,** 4511–4521
47. Feng, S., Chen, J. K., Yu, H., Simon, J.A., and Schreiber, S. L. (1994) Two binding orientations for peptides to the Src SH3 domain: development of a general model for SH3-ligand interactions. *Science* **266,** 1241–1247
48. Schwintzer, L., Koch, N., Ahuja, R., Grimm, J., Kessels, M. M., and Qualmann, B. (2011) The functions of the actin nucleator Cobl in cellular morphogenesis critically depend on syndapin I. *EMBO J.* **30,** 3147–3159
49. Pérez-Otaño, I., Luján, R., Tavalin, S.J., Plomann, M., Modregger, J., Liu, X. B., Jones, E. G., Heinemann, S. F., Lo, D. C., and Ehlers, M. D. (2006) Endocytosis and synaptic removal of NR3A-containing NMDA receptors by PACSIN1/syndapin1. *Nat. Neurosci.* **9,** 611–621
50. Griffon, N., Büttner, C., Nicke, A., Kuhse, J., Schmalzing, G., and Betz, H. (1999) Molecular determinants of glycine receptor subunit assembly. *EMBO J.* **18,** 4711–4721
51. Hirling, H. (2009) Endosomal trafficking of AMPA-type glutamate recep-

tors. *Neuroscience* **158,** 36–44
52. Kirsch, J., and Betz, H. (1995) The postsynaptic localization of the glycine receptor-associated protein gephyrin is regulated by the cytoskeleton. *J. Neurosci.* **15,** 4148–4156
53. Charrier, C., Ehrensperger, M.V., Dahan, M., Lévi, S., and Triller, A. (2006) Cytoskeleton regulation of glycine receptor number at synapses and diffusion in the plasma membrane. *J. Neurosci.* **26,** 8502–8511
54. Mammoto, A., Sasaki, T., Asakura, T., Hotta, I., Imamura, H., Takahashi, K., Matsuura, Y., Shirao, T., and Takai, Y. (1998) Interactions of drebrin and gephyrin with profilin. *Biochem. Biophys. Res. Commun.* **243,** 86–89
55. Giesemann, T., Schwarz, G., Nawrotzki, R., Berhörster, K., Rothkegel, M., Schlüter, K., Schrader, N., Schindelin, H., Mendel, R.R., Kirsch, J., and Jockusch, B.M. (2003) Complex formation between the postsynaptic scaffolding protein gephyrin, profilin, and Mena: a possible link to the microfilament system. *J. Neurosci.* **23,** 8330–8339
56. Kneussel, M., Brandstätter, J. H., Laube, B., Stahl, S., Müller, U., and Betz, H. (1999) Loss of postsynaptic GABA(A) receptor clustering in gephyrin-deficient mice. *J. Neurosci.* **19,** 9289–9297
57. Feng, G., Tintrup, H., Kirsch, J., Nichol, M.C., Kuhse, J., Betz, H., and Sanes, J.R. (1998) Dual requirement for gephyrin in glycine receptor clustering and molybdoenzyme activity. *Science* **282,** 1321–1324
58. Weltzien, F., Puller, C., O'Sullivan, G.A., Paarmann, I., and Betz, H. (2012) Distribution of the glycine receptor β-subunit in the mouse CNS as revealed by a novel monoclonal antibody. *J. Comp. Neurol.* **520,** 3962–3981